

International Conference on Space Optics—ICSO 2022

Dubrovnik, Croatia

3–7 October 2022

Edited by Kyriaki Minoglou, Nikos Karafolas, and Bruno Cugny,



Advanced concept of a photonic integrated circuit microlidar for navigation, landing and debris detection



Advanced concept of a photonic integrated circuit microlidar for navigation, landing and debris detection

Chrysovalantis Avraam^{*a}, Errico Armandillo^b, Tiago Sousa^c, Stavros Iezekiel^a, Georgios Charalambous^d, V. Kurtenoks^b, C. Ciminelli^e, D. Petrulionis^f, D. Stepanova^g

^aUniversity of Cyprus, Nicosia; ^bEventech, Riga; ^cEfacec; ^dUniversity of California, Davis; ^ePolitecnico di Bari; ^fAstrolight, Vilnius; ^gGOS (D)

ABSTRACT

LIDARs are considered a key enabling technology for an array of applications in space, including celestial body approach, landing, rendezvous and docking, space debris identification and CubeSat constellations. Reliability, low cost and low size, weight and power (SWaP) are critical factors for these applications. Current spaceborne LIDAR systems are based on discrete optical components. These systems consume a lot of power and are bulky. In this work, a hybrid integrated (FMCW) LIDAR system operating at 1550 nm and based on an indium phosphide (InP) and silicon nitride (Si₃N₄) platform along with an external erbium-doped fiber amplifier (EDFA) compact module is proposed. By using a telecom-wavelength laser with an ultra-narrow linewidth of 1 kHz, and a 1D optical phased array (OPA) using lead zirconate titanate (PZT) phase shifters, the proposed PIC microlidar can operate up to 100 km. In order to realize small beam divergence, a 1x100 linear array consisting of 4 mm Si₃N₄ dual-layer grating antennas with a coupling efficiency of up to 80% of the incident power is utilized.

Keywords: Spaceborne LIDAR, integrated LIDAR, FMCW LIDAR, photonic integrated circuits, hybrid integration, optical phased array, indium phosphide, silicon nitride, grating antennas

*Chrysovalantis Avraam, cavraa05@ucy.ac.cy

1. INTRODUCTION

Space photonics is a key enabling technology, with proven benefits for payloads and spacecraft in terms of system resources and functionalities when compared to traditional technologies, including: mass, harness reduction, electromagnetic interference (EMI) insensitivity, added functionalities, and broad bandwidths. In addition, photonics is the driving technology of spaceborne LIDAR instruments for an array of applications, including sensing, docking and rendezvous. In recent years, LIDAR technology has also been applied to commercial applications, notably autonomous navigation, where reliability, low cost and low size, weight and power (SWaP) are critical factors, and the bulky LIDARs typical of space are not suitable. In this regard, photonic integrated circuit (PIC) technology is seen as the way forward for automotive LIDAR requirements, with several designs already demonstrated and commercialized [1].

Planetary exploration represents one of the main activities of various space agencies, with missions to the Moon and Mars [2]. LIDARs are considered a key enabling technology for an array of applications, including celestial body approach and landing (Moon, Mars) providing hazard avoidance, rendezvous, docking, space debris identification and CubeSat constellations [3][4]. One of the key aspects of photonic integration is the different material platforms that are available, such as lithium niobate, silicon photonics, Si₃N₄, InP and heterogeneous integration. For automotive LIDAR, hybrid integration of both InP (for active transmitter/receiver portions) and Si₃N₄ (for passive optical phased arrays and optical power combining) is used.

Non-PIC LIDAR miniaturization efforts currently being addressed by ESA include the Miniaturized Imaging Laser Altimeter (MILA), a compact imaging altimeter for future missions, providing support for the global navigation system in the approach and landing of flying spacecraft [5], and LIDAR for Extraterrestrial Imaging Applications (LEIA), the landing LIDAR for ESA-Roscosmos' Luna-Resurs Mission [6]. Luna-Resurs is a joint ESA-Roscosmos mission to land at the Moon's south pole to search for minerals and water. A more recent development of relevance for micro-LIDARs is the NASA Kinematic Navigation and Cartography Knapsack (KNAck) project which aims to develop a portable LIDAR (in

collaboration with Aeva) that will eventually be mounted on astronaut backpacks and rovers for future lunar missions [7]. This employs an FMCW LIDAR in order to map the lunar terrain, producing a real-time map.

In the continued pursuit for miniaturization, integrated photonics is now under active consideration for space applications. PIC technology offers high levels of functionality and a potential path to co-integration with electronics and micro-optics. Given the legacy of 1550 nm technology for terrestrial data communications, InP-based PICs have been leveraged for photonic payloads. Apart from miniaturization, a key advantage of PIC technology is the development of optical phased arrays, which offer a robust non-mechanical approach to beam steering.

In this work, we present a hybrid integrated FMCW LIDAR based on InP-Si₃N₄, suitable for space applications. An ultra-narrow beam is diffracted in free space by using a 1x100 OPA based on Si₃N₄ platform which consists of 4 mm long waveguide grating arrays (WGA). InP is used for the active devices such as the intensity modulator and photodiode. The ultra-narrow linewidth (1 kHz) laser used in the system consists of two InP gain sections and two Si₃N₄ microring resonators (MRRs) in a Vernier configuration. The calculated coupling efficiency of the OPA is 0.84 at 1550 nm. Link budget analysis is performed and a signal to noise ratio (SNR) of more than 10 dB is obtained both for a single received pulse (10 km) and for 1000 integrated pulses (100 km).

The organization of the rest of the paper is as follows. The design methodology and system are described in Section 2. OPA performance and limitations are described in Section 3. The simulation results of the WGAs, far field patterns and link budget analysis are presented in Section 4.

2. APPLICATIONS REQUIREMENTS

The requirements for the applications aimed at in this work have been fully reviewed and assessed. The high-level system specifications are outlined in Table 1. These are initial values subject to iterations/updates as part of follow-on development activities.

Table 1: PIC-based micro-LIDAR high level initial performance specifications.

Requirement	Nominal Values	Goal Values
Operational Wavelength	1.5 μm	1.5 μm
Laser Power (CW)	~ 100 mW	~ 1 W
FoV No Scan	$< 3^\circ$ (TBD)	$< 0.5^\circ$ (variable TBD)
FoV with Scan	$< 10^\circ$ (TBD)	$< 5^\circ$
Measuring Distance	500 m – 8 km	100m – 20 km
Measuring Accuracy/Resolution	< 0.2 m (TBC)	< 0.5 m (TBC)
Velocity Range	50 m/sec (TBC)	< 100 m/sec
Velocity Resolution/Accuracy	< 2 m/sec (TBC)	< 2 m/sec (TBC)

3. SYSTEM DESCRIPTION

The conceptual diagram of our proposed PIC-based LIDAR is shown in Figure 1. The LIDAR system consists of the hybrid integration of InP and Si₃N₄ chips. The selection of these platforms is based on the fact that PICs based on InP cannot provide the waveguide power handling capability that is required for long-range LIDAR applications, while Si₃N₄ can handle several watts [8]. In contrast, the active photonic components (laser, modulator and photodiode) required for a LIDAR system cannot be designed in PICs based on Si₃N₄ [9], [10]. The first chip includes a laser (with two gain sections) coupled to a cavity in the Si₃N₄ platform, while the second chip includes the electro-absorption modulator (EAM), the optical power division network, the phase shifters, the grating antennas for the transmission and reception and the balanced photodiode. At the output of the modulator, an external EDFA is connected for in-line amplification between the InP and Si₃N₄ chips. An external Frequency Modulated Voltage-Controlled Oscillator (FM VCO) is used for FMCW operation.

A hybrid integrated laser consisting of two InP gain sections sharing a common laser mirror based on MMRs is used as shown in Figure 1. Using this configuration of cascaded MRRs an ultra-narrow Lorentzian linewidth of 1kHz can be achieved with an optical output power of 85 mW [11]. By increasing the number of gain sections, higher power levels can be achieved, but in our case, we are limited due to the modulator's low input power. This hybrid laser operates at a fixed wavelength of 1550 nm. FMCW operation can be achieved by keeping the operating wavelength of the laser fixed at 1550 nm and chirp-modulating its intensity with a VCO. The sweep rate of the chirped waveform is 1.3 kHz with a tuning frequency range between 10 and 20 GHz. In addition, since high optical output power is required for the proposed missions, an external compact module EDFA with a gain of 21 dB is connected at the output of the EAM for in-line amplification.

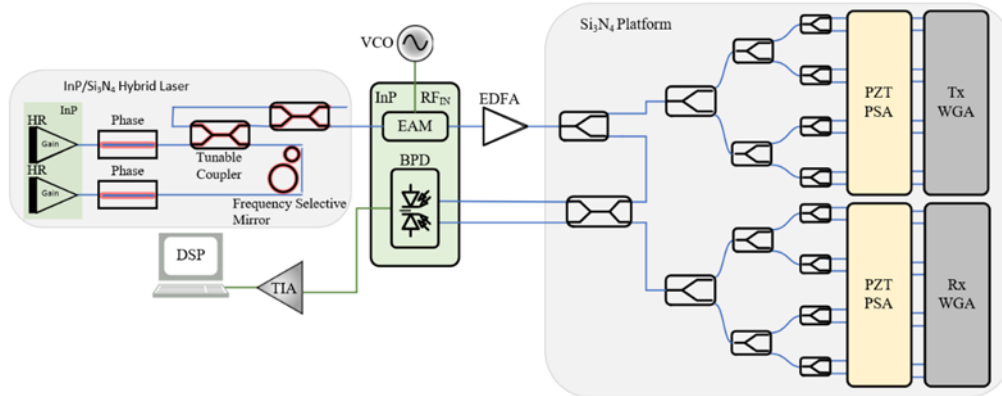


Figure 1. Conceptual diagram of FMCW PIC LIDAR based on InP/Si₃N₄.

Chirp nonlinearity is an important parameter that must be considered because it degrades the frequency of the system and the resolution of the range [4]. This nonlinearity depends on the dynamic response and the phase noise of the laser. Chirp nonlinearity can be reduced by various techniques, such as using phase-locked loops to suppress phase noise [5]. Due to the ultra-narrow linewidth of the laser, it is not expected to have a large variation over its lifetime with regard to the relation between the VCO voltage and the emission wavelength. Moreover, this relation is expected to be linear over the expected working range.

After the chirped light passes through the EDFA, it is split into two paths; one is transmitted to free space through the waveguide grating antennas towards the target, while the other serves as the LO input to the coherent receiver. The reflected light from the target is interferometrically recombined with the reference LO and they pass through the balanced photodiode (BPD). In LIDAR systems, noise can be a large problem since we are dealing with low-power received signals. Using balanced photodetection, this problem can be eliminated by detecting the differences between the two input signals and simultaneously suppressing the fluctuations.

Using the FMCW technique, the range and velocity of the object can be calculated simultaneously by measuring the beat and Doppler frequency. Figure 2 illustrates a chirped signal, where the blue line indicates the FM transmitted signal while the red line shows the received signal shifted by Δt . By mixing these two signals, two beat frequencies are produced f_{b1} and f_{b2} on the upchirp and downchirp side, respectively. The range and relative velocity can be calculated from equations (1) and (2), where T is the chirped period, c is the speed of light and B is the chirped bandwidth:

$$R = \frac{T_c}{2B} \frac{f_{b1} - f_{b2}}{2} \quad (1)$$

$$v = \frac{1}{2} \frac{f_{b1} + f_{b2}}{2} \quad (2)$$

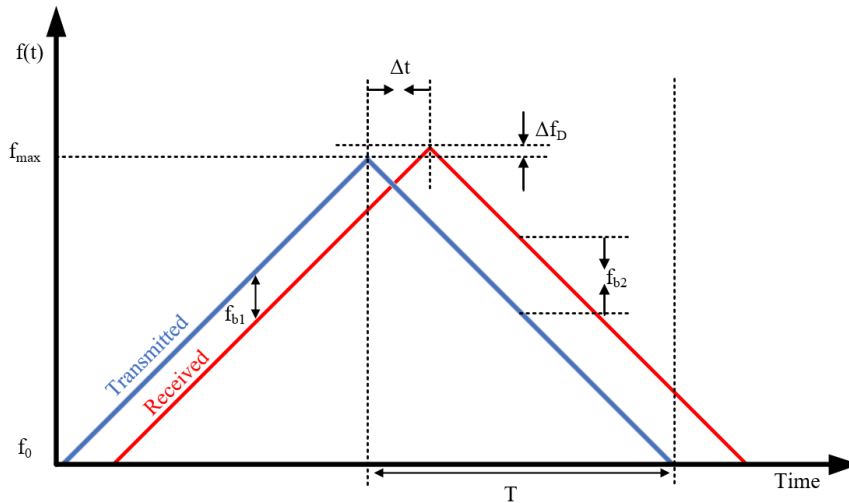


Figure 2. Linear chirp modulation of a signal and the beat frequencies it produces through interference between the transmitted and received light.

4. OPTICAL PHASED ARRAY

The most challenging part of our LIDAR system is the OPA. Current OPAs are based on mechanical beam steering, providing high resolution and large Field-of-View (FoV), but they are bulky, limited in speed and consume a lot of power [14]. In recent years, integrated OPAs have attracted significant attention for beam shaping and beam steering, since using this technology allows narrow beam width, high steering speed and low SWaP requirements to be achieved [15]. The key components of an integrated OPA are the WGAs, phase shifters, and the optical power division network (OPDN) as shown in Figure 3.

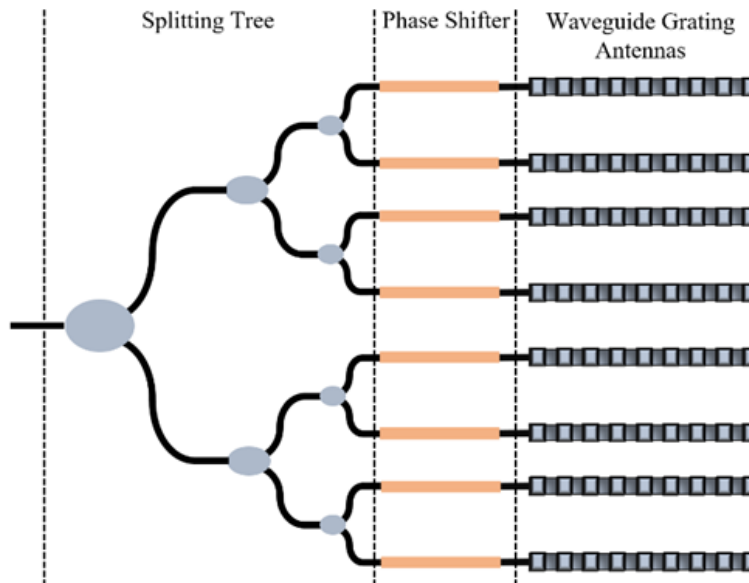


Figure 3. Key components of an integrated OPA.

The footprint of the OPDN will have a significant effect on the far-field properties of the OPA. The arrangement of the OPDN and type of the beam splitter to be used defines the number of WGAs in the array. The steering angle and the divergence of the beam are directly related to the aperture of the OPA as seen in Equation (3):

$$D\varphi = \frac{0.886\lambda_0}{Nd \cos(\varphi_{\text{steer}})} \quad (3)$$

Here, N is the number of the antenna elements in the array, d is the pitch between each antenna element and φ_{steer} is the steering angle. In the case where the aperture of the OPA decreases, which means that the pitch of the waveguide decreases, the scanning angle increases, especially when the pitch is less than the operating wavelength [2]. In addition, when the waveguide pitch decreases, the divergence of the beam in the far-field increases, thus degrading the resolution of the LIDAR.

By increasing the number of antenna elements and keeping the pitch small, large beam steering angles and small beam divergence can be achieved. Furthermore, to feed a large number of antennas in the array, a large number of splitting units will be needed for equal input power distribution into each output channel. Therefore, the splitting unit must be carefully selected to avoid any degradation in the performance of the OPA. Multimode interference (MMI) splitters, star couplers, Y-branch splitters and directional couplers can be used to implement the OPDN. In our case, Y-branch splitters are used to utilize the OPA. Another important parameter that must be considered is the optical crosstalk between the adjacent waveguides. When the spacing between the adjacent waveguides (or pitch) is small, phase and amplitude modulation is prevented between the waveguides. When the waveguides are spaced a few micrometres apart, crosstalk between adjacent waveguides is minimized, at the expense of steering range.

Most integrated OPAs reported are based on the thermo-optic (TO) effect [16],[17]. The TO phase shifter varies the temperature of the waveguide via current control. As a result, this change in temperature will change the refractive index of the waveguide material, which, in turn, will modify the phase of the light. In the case of Si_3N_4 , the thermo-optic coefficient is in the range of $2-4 \times 10^{-5} \beta_{\text{TO}}/\text{K}$ which is low and leads to increase power consumption, a larger phase shifter and limits the beam steering speed [15]. Using the Si_3N_4 platform for the implementation of thermo-optic modulators in the OPA, the power consumption will be of the order of 400 mW per π phase shift per modulator, which is relatively high in the case of large-scale waveguide arrays, especially for LIDAR applications. To circumvent this limitation, low power and high-speed actuators using piezo-electric materials were adopted. Lead zirconate titanate (PZT) is deposited on top of the Si_3N_4 waveguide [18]. When this piezo-electric material is exposed to an electric field by biasing an electrode, the PZT expands in the direction along the electric field and contracts in the other directions, leading to variation of the optical phase. When WGAs are placed in one dimension in space, two-dimensional beam steering can be achieved. The lateral direction is steered by manipulating the phase, while the longitudinal direction is steered by adjusting the operating wavelength. Our OPA is limited to the lateral direction since the WGAs have small beam steering efficiencies in the range of 0.1 to 0.2°/nm. For example, to achieve a steering range of 8° in the longitudinal direction, a tunable laser with 40 nm wavelength bandwidth is needed. As seen from Equation (1), the beat frequency for the range depends on the chirp period and the chirp bandwidth. Assuming that we want to detect a target at 100 km range with a chirp period of 100 μs and chirp bandwidth of 40 nm (11 THz), this leads to a beat frequency equal to 266 GHz, which is far beyond the bandwidth offered by PIC photodiodes and is in fact only feasible if photomixers are used.

Two common types of grating antenna are usually used for the radiation of the optical beam in integrated OPAs, arc and straight WGAs [19], [20]. The radiation properties and structure of the grating antenna have a significant effect on the far-field properties. Since large beam steering angles are required, a straight WGA is the most suitable type of antenna due to the narrow linewidth of the beam. By increasing the length of the grating, wider beam steering angles can be achieved. The most important parameters for the grating antenna in the case of FMCW LIDAR are the coupling efficiency or radiation efficiency, the diffraction angle, and the beam divergence. In designing a WGA, some restrictions must be followed. For example, some parameters are determined by the wafer type that will be used (the thickness of the Si_3N_4 layer and the thickness of the substrate). Other parameters such as the etch depth and the duty cycle are dependent on the fabrication process. With single layer grating antennas, a bidirectional radiation pattern is generated, which degrades the coupling efficiency in the upward direction, since some of the light is going downward to the substrate. In this case, coupling efficiencies of 60-70% can be achieved. To prevent this limitation, dual-layer Si_3N_4 WGAs were used.

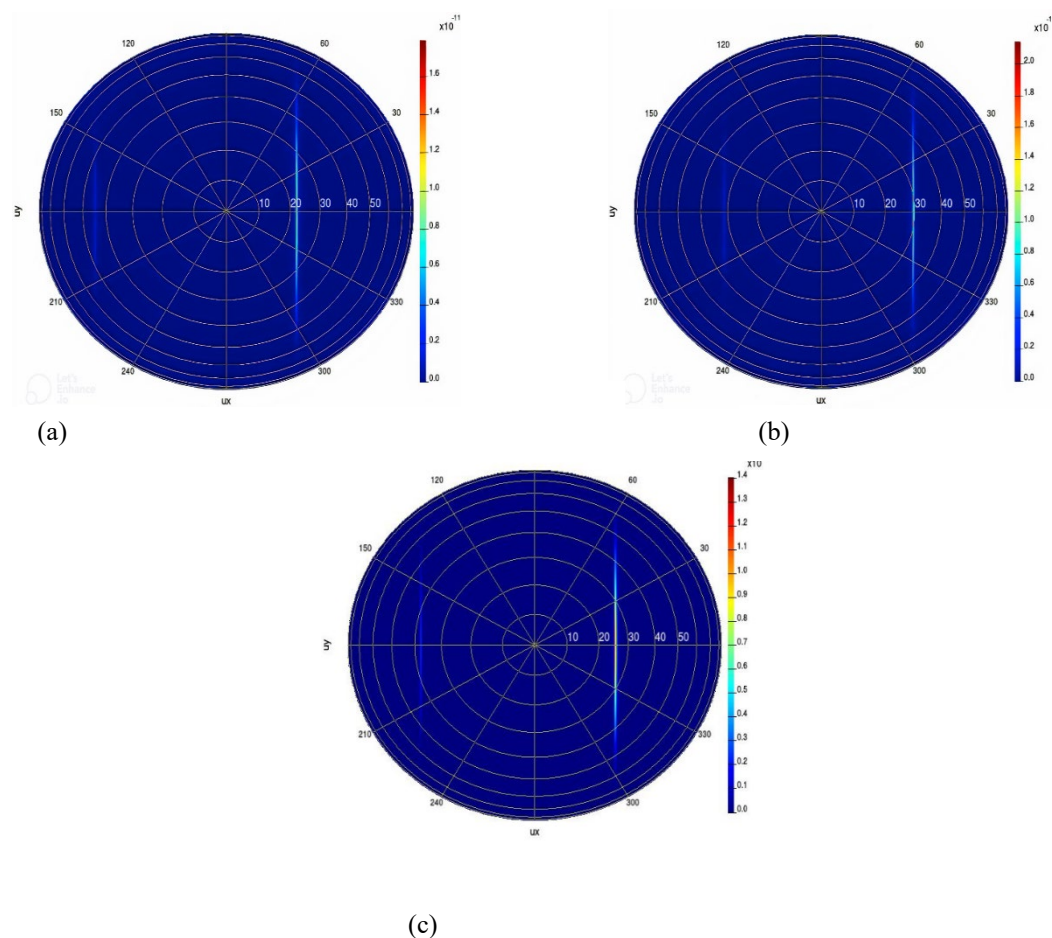


Figure 5. Far field of a single antenna element in upward direction at different wavelengths (a) 1500 nm, (b) 1600 nm, and (c) 1550 nm.

For microwave antennas the far-field pattern or radiation pattern of an antenna array is determined by the product of the array factor and the element factor (radiation pattern of a single antenna). This can also be applied in the case of optical antennas [23]. In an OPA, the distance between the adjacent antennas must be selected carefully. The antenna spacing determines the location of the grating lobes in the far-field pattern. The grating lobes will limit the beam steering range of the OPA and degrade the intensity of the main lobe. Ideally, a pitch of $\lambda/2$ is optimal to avoid grating lobes, but this small spacing between the antennas leads to optical crosstalk. By increasing the spacing between the adjacent waveguides to reduce optical crosstalk, the beam divergence increases simultaneously, and the beam steering range decreases. To reduce crosstalk and have a small beam divergence and a large beam steering range, we should keep the antenna spacing at an optimal value and increase the number of antennas (large-scale array). To evaluate the far-field properties of the OPA, we simulated a 1×100 array of grating antenna elements by arranging them linearly in one dimension for the y-axis. The spacing between the adjacent waveguides is $1.1 \mu\text{m}$. Figures 7 (a) and (b) show the simulated far-field patterns of the array at azimuth and elevation cut, respectively. As seen, for both patterns, the grating lobes are well suppressed.

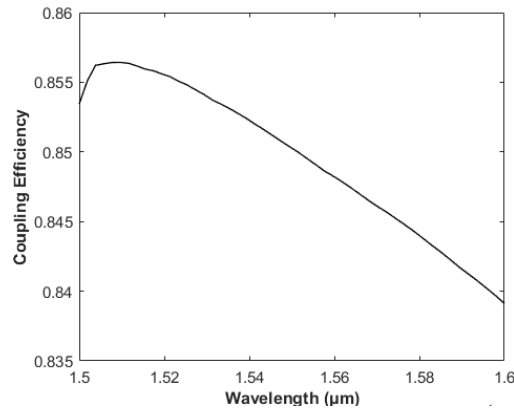


Figure 6. Coupling efficiency of the WGA with variation of wavelength.

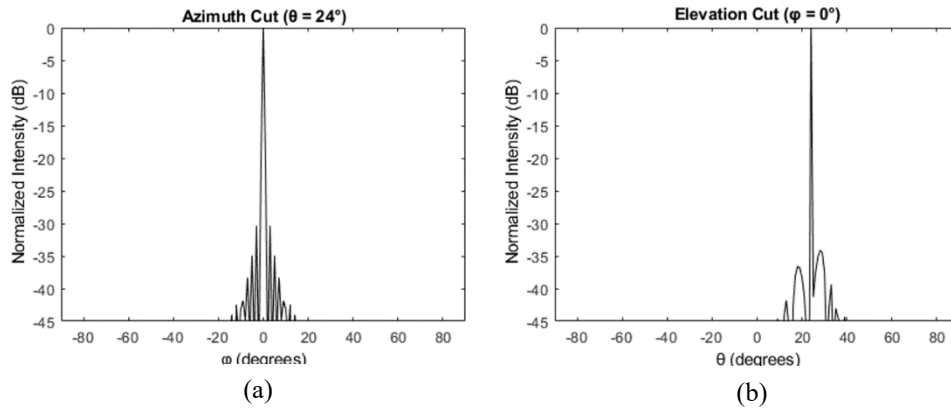


Figure 7. Simulated far field of 1x100 linear array of WGAs, (a) azimuth cut at $\theta = 24^\circ$, and (b) elevation cut at $\varphi = 0^\circ$.

5.2 Link Budget analysis

For a LIDAR system the most important parameters that must be considered for long distances are the laser power, beam divergence, receiver aperture, SNR and coupling efficiencies for chip-to-free-space and vice versa. Using the LIDAR range equation, and considering the above parameters, the maximum operating range can be calculated. There are many variations of the range equation, each depending on the expected use. Equation (4) relates the absorption coefficient of the transmission medium, target reflectance, beam divergence and the parameters of the system.

$$P_R = P_T (1 - q) g \frac{D_{rec}^2}{4R^2} \cos(j) e^{-2\alpha R} \eta_{sys} \quad (4)$$

Here, P_R is the return signal from the target, P_T the transmitted power, θ the beam divergence in mrad, γ the reflectivity of the target, φ the incident angle of the returned signal, D_{rec} the receiver aperture, α the absorption coefficient of the medium and η_{sys} the system losses. The main factor that affects the returned power is the range R , since the inverse-square relation leads to a rapid reduction in optical power with increasing range. To compensate this loss, a larger receiver aperture must be used. Based on the diagram of Figure 1 and on the performance parameters of Table 2, a link budget analysis is performed. A laser with output optical power of 85 mW is modulated by a chirped RF signal. The FM optical signal is amplified by a SOA with a gain of 21 dB. Including the coupling losses from chip-to-chip, the resulting optical power

before the splitter is 34.2 dBm. Subsequently, the modulated optical signal is divided into two paths. One is sent to the grating antenna array for transmission, while the other portion is used as the LO. By including the losses of the splitting tree, OPA and of the grating antennas, the resulting free-space optical power is found to be 1.072 W. The LO power is set to 50 mW to ensure that the shot noise limit is reached, in order to improve the SNR. Interference signals are detected by a balanced photodetector with a bandwidth of 45 GHz. The frequency sweep period of the VCO is set to 1.3 kHz with a frequency tuning bandwidth of 10 GHz. Figure 8 shows the SNR versus range for a single received pulse and 1000 integrated pulses before mixing with the LO on the BPD of our proposed LIDAR system. In the case of single-pulse homodyning, good SNR is achieved up to a few tens of km. In this case, maximum performance is achieved for range and velocity resolution when $\Delta R = 1.5$ cm (range resolution) and $\Delta U = c\Delta n/B$ (relative velocity resolution), respectively. Here, Δn is the laser linewidth. The maximum relative velocity (U) of the target is 15 km/sec. By integrating the received train of backscattered pulses, the maximum range scale is \sqrt{N} , where N is the number of integrated pulses, while the range accuracy increases linearly with N . The velocity values do not change significantly as they depend mostly on the chirp BW. Table 3 and Figure 8 summarizes the system specifications and simulation results in FM mode.

Table 3. LIDAR link budget performance parameters.

Transmitter	Wavelength	1550 nm
	Laser Output Power	1 W
	Chirped Period	1.3 kHz
	Chirped Bandwidth	10 GHz
	Local Oscillator Power	50 mW
	Beam Divergence	2.6 mrad (0.15°)
Receiver/Detector	WGA Aperture	4 mm
	Dark Current (I_D)	25 nA
	Responsivity	1 A/W
	Bandwidth	45 GHz
System Losses	Splitting Tree	1 dB
	Phase shifter array	2 dB
	Chip-to-Chip CL	1 dB
	Free-space coupling losses	0.7 dB
Atmosphere/Target	Atm. Coefficient (km^{-1})	0
	Target Reflectivity	0.01
	Background Irradiance	0.1 W/nm/m ²

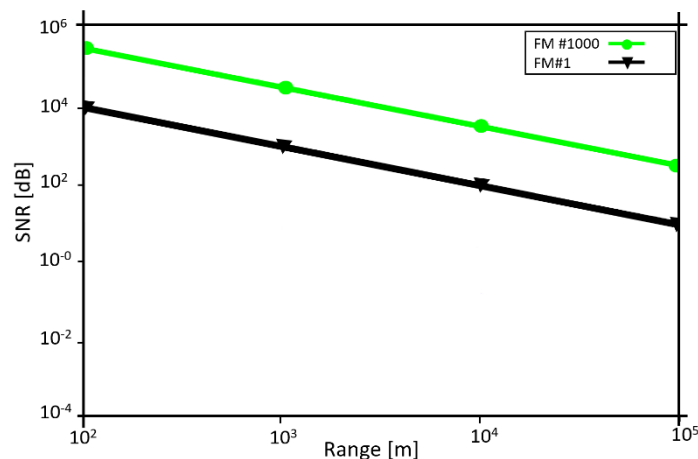


Figure 8. SNR versus range for a single received pulse and 1000 integrated pulses.

6. CONCLUSIONS

Within this study we have shown by analysis and simulations that a novel concept of a hybrid integrated (FMCW) LIDAR system, operating at 1550 nm and based on the indium phosphide (InP) and silicon nitride (Si₃N₄) platforms along with an external erbium-doped fiber amplifier (EDFA), is capable of replacing non-PIC micro-LIDARs in a number of space ranging applications. The concept explored and assessed here represents a step forward in the operability of PIC-based technologies towards spaceborne applications that today are exclusively the domain of larger systems. Preliminary simulation results and analysis have indicated that the proposed hybrid PIC micro-LIDAR can operate up to 100 km. A breadboarding activity to verify the results of this study is in the process of being initiated within the UCY Photonics group.

ACKNOWLEDGMENTS

This work is partially financed by ESA under PECS Cyprus and Lithuania contracts.

REFERENCES

- [1] SiLC, "First Commercially Available Chip-Integrated FMCW LiDAR Sensor", 2022, <https://www.silc.com/product/> (Accessed 20 August 2022).
- [2] Mango, D., Opromolla, R. and Schmitt, C., "Hazard detection and landing site selection for planetary exploration using LIDAR". IEEE 7th International Workshop on Metrology for AeroSpace (MetroAeroSpace), (2020).
- [3] Mamani, J. and Cardenas, P., "LiDAR small satellite for space debris location and attitude determination". IEEE International Conference on Aerospace and Signals (INCAS), (2019).
- [4] Pierrottet, D., Amzajerdian, F., Hines, G., Barnes, B., Petway, L. and Carson, J., "Lidar Development at NASA Langley Research Center for Vehicle Navigation and Landing in GPS Denied Environments". IEEE Research and Applications of Photonics In Defense Conference (RAPID), (2018).
- [5] Pollini, A., Pache, C. and Haesler, J., "CSEM Space Lidars for Imaging and Ranging". IGARSS 2018 - 2018 IEEE International Geoscience and Remote Sensing Symposium, (2018).

-
- [6] Bradshaw, M., "LEIA: THE LANDING LIDAR FOR ESA-ROSCOSMOS LUNARESURS MISSION", 2017, <https://iafastro.directory/iac/archive/browse/IAC-17/A3/2B/38290/> (accessed 20 August 2022).
- [7] Porter, M., "NASA, Partners Develop Lunar Backpack Technology to Aid New Moon Explorers", 2022 <https://www.nasa.gov/centers/marshall/news/releases/2022/nasa-partners-develop-lunar-backpack-technology-to-aid-new-moon-explorers.html> (Accessed 20 August 2022).
- [8] Zhang, L., Li, Y., Hou, Y., Wang, Y., Tao, M., Chen, B., Na, Q., Li, Y., Zhi, Z., Liu, X., Li, X., Gao, F., Luo, X., Lo, G. and Song, J., "Investigation and demonstration of a high-power handling and large-range steering optical phased array chip". *Opt. Express* 29, 29755-29765, (2021).
- [9] Rahim, A., Goyvaerts, J., Szelag, B., Fedeli, J., Absil, P., Aalto, T., Harjanne, M., Littlejohns, C., Reed, G., Winzer, G., Lischke, S., Zimmermann, L., Knoll, D., Geuzebroek, D., Leinse, A., Geiselman, M., Zervas, M., Jans, H., Stassen, A., Dominguez, C., Munoz, P., Domenech, D., Giesecke, A., Lemme, M. and Baets, R., "Open-Access Silicon Photonics Platforms in Europe". *IEEE Journal of Selected Topics in Quantum Electronics*, 25(5), pp.1-18, (2019).
- [10] Smit, M., Wale, M., Van der Tol, J., Leijtsens, X., Grote, N., Ambrosius, H., Schell, M., Robbins, D. and Bente, E., "A Generic foundry model for InP-based photonics". *IET Optoelectronics*, 5(5), pp.187-194, (2011).
- [11] Epping, J., Oldenbeuving, R., Geskus, D., Visscher, I., Grootjans, R., Roeloffzen, C. and Heideman, R., "High power, tunable, narrow linewidth dual gain hybrid laser", *Laser Congress 2019 (ASSL, LAC, LS&C), OSA Technical Digest (Optica Publishing Group), paper ATu1A.4*, (2019).
- [12] Zhang, A., Xiaosheng, T., "Laser Chirp Linearization and Phase Noise Compensation for Frequency-modulated Continuous-wave LiDAR", Master's Thesis, IEECS Department, University of California, Berkeley, (2021).
- [13] Behroozpour, B., Sandborn, P., Quack, N., Seok, T., Matsui, Y., Wu, M. and Boser, B., "Electronic-Photonic Integrated Circuit for 3D Microimaging". *IEEE Journal of Solid-State Circuits*, 52(1), pp.161-172, (2017).
- [14] Guo, Y., Guo, Y., Li, C., Zhang, H., Zhou, X. and Zhang, L., "Integrated Optical Phased Arrays for Beam Forming and Steering". *Applied Sciences*, 11(9), p.4017, (2021).
- [15] Sun, X., Zhang, L., Zhang, Q. and Zhang, W., "Si Photonics for Practical LiDAR Solutions". *Applied Sciences*, 9(20), p.4225, (2019).
- [16] Jie Sun, Timurdogan, E., Yaacobi, A., Zhan Su, Hosseini, E., Cole, D. and Watts, M., "Large-Scale Silicon Photonic Circuits for Optical Phased Arrays". *IEEE Journal of Selected Topics in Quantum Electronics*, 20(4), pp.264-278, (2014).
- [17] Tao, M., Peng, T., Ding, C., Guan, J., Li, Y., Zhang, L., Chena, B., Gao, L., Li, X., Song, J. and Gao, F., "A Large-Range Steering Optical Phased Array Chip and High-Speed Controlling System". *IEEE Transactions on Instrumentation and Measurement*, 71, pp.1-12, (2022).
- [18] Casset, F., "Stress optic modulator using thin-film PZT for LIDAR applications", *IEEE Sensors*, pp. 1-4, (2019).
- [19] Gad, M., Zaki, A. and Sabry, Y., "Silicon photonic mid-infrared grating coupler based on silicon-on-insulator technology". *34th National Radio Science Conference (NRSC)*, (2017).
- [20] Im, C., Bhandari, B., Lee, K., Kim, S., Oh, M. and Lee, S., "Silicon nitride optical phased array based on a grating antenna enabling wavelength-tuned beam steering". *Optics Express*, 28(3), p.3270, (2020).
- [21] Cheng, L., Mao, S., Li, Z., Han, Y. and Fu, H., "Grating Couplers on Silicon Photonics: Design Principles, Emerging Trends and Practical Issues. *Micromachines*", 11(7), p.666, (2020).
- [22] Poulton, Christopher Vincent, "Integrated LIDAR with optical phased arrays in silicon photonics", 2016, Master Thesis, <https://dspace.mit.edu/handle/1721.1/110868> (Accessed 20 August 2022).
- [23] Balanis, C., n.d. "*Antenna Theory: Analysis and Design*", 4th edition, (2016).